

Energy Absorption of a Novel Lattice Structure-Filled Multicell Thin-Walled Tubes Under Axial and Oblique Loadings

Gazi Basar Kocabas,* Senai Yalcinkaya,* Erhan Cetin, and Yusuf Sahin

Multicell design and lattice structure as filling material are two effective methods for enhancing the energy absorption performance of thin-walled tubes. This study combines these two approaches to present a multicell tube with a novel lattice structure and investigates the energy absorption performances of these hybrid multicell tubes under axial (0°) and oblique (10°, 20°, and 30°) impact loading conditions. As filling structure, β -Ti₃Au lattice geometry with varying lattice strut diameters and the number of lattice unit cells are used, while the single and multicell thin-walled tubes with different tube thicknesses are employed as main absorbing element. In this context, the effects of numbers of lattice unit cells, lattice strut diameter, cell numbers of the tube, and tube thickness on energy absorption performance of hybrid tubes are examined using validated nonlinear finite element models. This investigation unveils that the synergistic interplay between the multicell tubes and lattice structure during deformation significantly elevates the energy absorption performance of the hybrid structure. Notably, the findings demonstrate that multicell hybrid tubes exhibit a remarkable capacity to absorb up to 30.36% more impact energy compared to the aggregate absorption of individual components in hybrid tubes.


tubes,^[6] researchers examined hexagonal,^[7] octagonal,^[8] hat-shaped^[9,10] and conical^[11] structures, increasing the impact resistance of thin-walled tubes by changing the cross-sectional shape. Recently, a great deal of research has been done to enhance the crashworthiness performance of thin-walled structures—particularly thin-walled multicell tubes, which have garnered a lot of interest because of their exceptional energy absorption (EA) qualities and low weight. Gao and Ruan^[12] proposed two types of hierarchical multicell square tubes and crashworthiness performances of the tubes having different hierarchical orders and wall thickness were studied numerically. Inspired by the cross-sectional properties of bamboo, Zu et al.^[13] proposed a novel thin-walled multicell tube, and the axial, lateral, and bending properties of these structures were examined using the finite element (FE) method.

Researchers have been trying various ways to further improve the deformation stability and therefore the crashworthiness performance of thin-walled tubes. These may take the form of strengthening the outer part of thin-walled tubes with various materials such as composites or filling the inner part of the tubes with polymer or metallic materials.^[1,2,14–16] For instance, Bai et al.^[17] proposed single tubes filled with body-centered cubic (BCC) lattice structure produced by additive manufacturing (AM) technology. Integrated AlSi10Mg lattice and single tubes subjected to quasistatic

1. Introduction

The crash boxes, which are generally used in the form of the metal thin-walled tubes used in vehicles, convert the kinetic energy occurring during the accident into plastic deformation energy. Significant attempts have been made to better understand the crushing characteristics of thin-walled structures by employing analytical, numerical, and experimental methods.^[1–4] No longer sticking to the general circular^[5] and square

G. B. Kocabas
Department of Machine and Metal Technologies, Technical Sciences
Vocational School
Istanbul Arel University
Istanbul 34295, Türkiye
E-mail: gazibasarkocabas@arel.edu.tr

 The ORCID identification number(s) for the author(s) of this article can be found under <https://doi.org/10.1002/adem.202400483>.

© 2024 The Author(s). Advanced Engineering Materials published by Wiley-VCH GmbH. This is an open access article under the terms of the Creative Commons Attribution-NonCommercial-NoDerivs License, which permits use and distribution in any medium, provided the original work is properly cited, the use is non-commercial and no modifications or adaptations are made.

DOI: 10.1002/adem.202400483

S. Yalcinkaya
Department of Mechanical Engineering, Faculty of Technology
Marmara University
Istanbul 34840, Türkiye
E-mail: syalcinkaya@marmara.edu.tr

E. Cetin
Department of Mechanical Engineering, Faculty of Engineering
Hitit University
Çorum 19030, Türkiye

Y. Sahin
Department of Mechanical Engineering, Faculty of Engineering
Ostim Technical University
Ankara 06374, Türkiye

compression loading were investigated both experimentally and numerically. Similarly, Tao et al.^[18] proposed one-piece printing and split-printing hybrid tubes, and EA performance and deformation mode of the tubes under axial and transverse loading were compared by experiments and numerical approaches. The EA properties of truncated metallic conical sandwich shells filled with polymeric foam and featuring corrugated cores were carefully examined under axial compression by Yang et al.^[19] Liu et al.^[20] proposed the use of chopped carbon fiber-reinforced polyamide to create 3D printed lattice-filled multicell tubes. The compression responses and EA characteristics of multicell tubes were investigated via quasistatic compression testing. Güler et al.^[21] examined the EA performance of multicell tubes filled with Al foam, and the mean crush force (MCF) of foam-filled hybrid tubes was predicted using a theoretical model that considers the foam, the tube, and their combined effects. Liu et al.^[22] proposed a novel multi cell thin-walled tube filled with uniform and graded BCC lattice structures, utilizing the benefits of multi cell tubes and lattice structures in increased crashworthiness performance.

As seen from the aforementioned studies, most of the published research on thin-walled tube crushing exclusively discusses axial loading. However, loading in real-world impact loading scenarios—most notably, car crashworthiness—is rarely entirely axial; instead, it frequently includes off-axis or oblique loads. A combination of global bending (Euler) collapse modes and axial bending leads the thin-walled tube to deform under such strain. It is crucial to comprehend how these energy absorbers react to oblique loading as a result.^[23] On the other hand, in the literature, studies examining the EA performance of multicell tubes under oblique loading are limited. Some of the studies conducted are summarized. The design strategy of a CFRP/Al hybrid multicell tube with variable thickness under multiangle compression loading was studied by Liang et al.^[24] Ha et al.^[25] suggested creating new hierarchical multicell bitubular tubes that are bioinspired and resemble natural tree forms. Through numerical analysis, the EA capacities of the structures with interior diameters and hierarchical ordering were examined under various loading angles. In addition, the mean crushing force of the suggested tubes was calculated theoretically using the simplified super-folding element theory. Zeng et al.^[26] examined the crashworthiness of multicell tubes with different structures under axial and oblique impact loads and suggested a novel design approach for multicell thin-walled tubes, which was motivated by the “cake-cutting” problem. By Huo et al.^[27] the crashworthiness of a thin-walled tube with equal gradient thickness variation under axial and oblique loading conditions was investigated using nonlinear FE analysis. Li et al.^[28] compared the EA capabilities of functionally graded thickness, tapered uniform thickness, and widely utilized straight uniform thickness tubes subjected to oblique impact loading.

Motivated by the above literature studies, material-filled thin-walled tubes can greatly improve EA applications in a variety of sectors. They increase the crashworthiness and impact resistance of automobiles and aircraft in the automotive and aerospace industries. Enhanced safety in collisions is advantageous for both rail and maritime transportation. Sports gear, such as bike frames and helmets, is better able to withstand hits. Bridges and structures resistant to earthquakes are examples of civil

engineering applications. Ballistic protection and armored vehicles are examples of military applications. While consumer devices are becoming more resistant to drops, sports bags and luggage are becoming more robust. These structures safeguard mechanical components in robots by reducing vibration and damage. These many uses highlight the wide range of possibilities for hybrid energy-absorbing structures.

To the best of our knowledge, there is no study on the crashworthiness performance of multicell hybrid thin-walled tubes under oblique loading conditions. Therefore, in this study, the EA performances of hybrid multicell tubes were examined under axial and oblique loads. In this context, a novel lattice structure geometry (i.e., β -Ti₃Au geometry) has been proposed as a filling material for the thin-walled tubes. In our previous study,^[29] we proposed β -Ti₃Au lattice structure for the first time in the literature to increase the EA performance of single thin-walled tubes and tested experimentally these structures under axial loads. The previous study revealed that the proposed lattice structure geometry has a more promising potential compared to traditional lattice structures such as face-centered cubic and BCC. At this point, the number of lattice unit cells, lattice strut diameter, cell numbers of the tube, and tube thickness were considered as design parameters, and crashworthiness performances of the multicell hybrid tubes were examined under both axial (0°) and oblique (10°, 20°, and 30°) impact loading conditions.

2. Experimental Section

2.1. Key Crashworthiness Index

As in refs. [15,29–34], some crashworthiness indicators can be used to quantitatively evaluate the crashworthiness properties of the hybrid tubes. These criteria are summarized below.

EA: EA represents the total energy absorbed throughout the crushing process, which can be computed as follows

$$EA = \int_0^{\delta} F(x) dx \quad (1)$$

where δ represents the crushing distance and $F(x)$ denotes the instantaneous crushing force.

Specific energy absorption (SEA): The absorbed energy of the crushing tube per unit mass is denoted by SEA and can be computed as follows

$$SEA = \frac{EA}{m} \quad (2)$$

where m denotes the mass of the multicell hybrid tube.

MCF: MCF is defined as the ratio of the EA to the crushing distance (δ), and can be calculated as

$$MCF = \frac{EA(\delta)}{\delta} \quad (3)$$

Peak crush force (PCF): PCF is the maximum crushing force during the crushing process. In most cases, the PCF value is at the beginning of the force–displacement curve, in which case it is called initial crush force (ICF). EA, SEA, and MCF values are expected to be as high as possible.^[35] On the other hand, in order

to protect passenger safety and prevent structural damage, the ICF value should be reduced as much as possible, taking into account the total EA value. On the contrary, in some cases, PCF is at the end of the force–displacement curve (i.e., at the densification region).^[3,30]

Crush force efficiency (CFE): CFE is defined as the ratio of the MCF to PCF, and can be obtained by

$$CFE = \frac{MCF}{PCF} \quad (4)$$

CFE is a measure of the stability of the crushing force value and is desired to be as close to 1 as possible.

Furthermore, the crush efficiency (CE) is defined as the maximal crush length per initial tube length (L) and is expressed as

$$CE = \frac{\delta}{L} \quad (5)$$

When the force–displacement curves after the crushing process were analyzed in this study, it was found that the majority of the multicell tubes considered entered the densification region after around 70% of the tubes. Therefore, the CE value was chosen as 0.70 for all tubes.

2.2. Geometric Description

The thin-walled multicell tubes are enhanced by β -Ti₃Au lattice structures in this study. Inspired by studies in the literature,^[36,37] the lattice structures were designed using Solidworks program. The designed single unit cell of β -Ti₃Au lattice structure and multicell hybrid tube are presented in **Figure 1**. At this point, number of cell, number of lattice unit cells per structure, lattice strut diameter, and tube thickness were considered as design parameters. Three different types of each design parameter were selected. The proposed design parameters are presented in **Table 1**.

The external dimensions of β -Ti₃Au lattice structures are $20 \times 20 \times 20$ mm, and height of the thin-walled tube is 100 mm. Due to their geometric compatibility with the proposed β -Ti₃Au lattice structures, square thin-walled tubes were used in all designs. The desired structures were obtained by multiplying the unit lattice structures (as shown in Figure 1) in the vertical

Table 1. Proposed structures and design parameters.

Parameter	Level 1	Level 2	Level 3
Number of cells for tubes	1 × 1	2 × 2	3 × 3
Number of lattice unit cells per structure	4	5	6
Lattice strut diameter, mm	1	2	3
Tube thickness, mm	0.5	1	1.5

direction. In addition, it should be mentioned that the members of the lattice structures are considered to be completely straight and to have a constant diameter when they are modeled using an idealized structural geometry.

2.3. FE Model

2.3.1. FE Modeling for Crash Simulations

FE simulations were performed to evaluate the crashworthiness performance of proposed single and multicell tubes by using ABAQUS/Explicit software. 4-node linear shell elements with reduced integration (S4R) were employed for the single and multicell tubes, 8-node linear brick elements with reduced integration (C3D8R) were used for the β -Ti₃Au lattice structures, and 4-node linear quadrilateral elements (R3D4) were employed for fixed and rigid plates. The hybrid structures were positioned between two rigid walls, the bottom of which is fixed and the top is movable. The loading angles between the multicell hybrid tube and rigid wall, θ , are 0°, 10°, 20°, and 30°. The upper movable wall, which was allowed to move only vertically, was given a speed of 10 m s^{-1} with a mass of 500 kg. General contact property was defined for all interactions between rigid plates, tubes, and lattice structures. A friction coefficient of 0.2^[38–40] was used by using the penalty formulation to describe the tangential behavior between all contacts, and “hard” contact was defined as the contact interaction characteristic to describe normal behavior. In addition, the upper surface of the hybrid structures and the lower surface of the movable plates were connected to each other with the “tie” command by establishing a master–slave relationship. The edge of the moving rigid plate is assigned a reference point to record the displacement, and the edge of the fixed rigid plate is assigned a reference

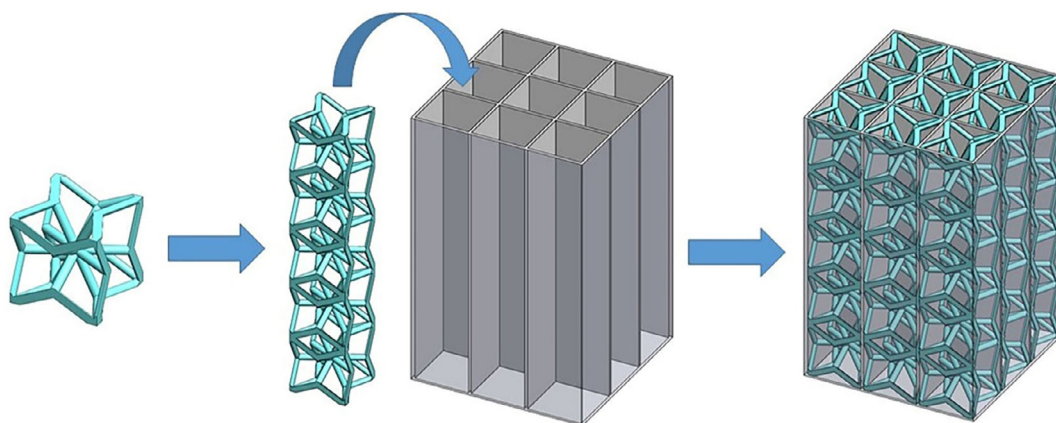


Figure 1. The schematic view of the single unit cell of β -Ti₃Au structure and the multicell hybrid tubes.

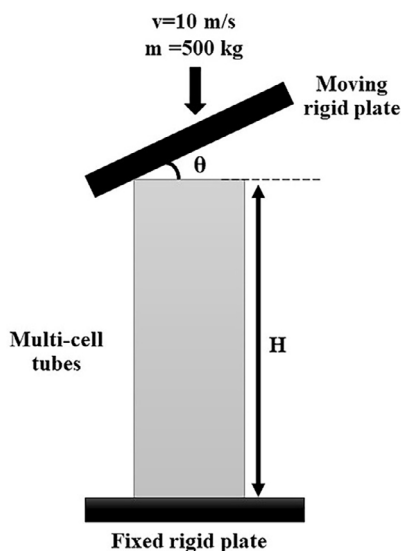


Figure 2. The FE model of the multicell hybrid tubes under oblique loading condition.

point to record the reaction force. As there was no obvious fracture seen in the experiments, failure criteria were not included in the FE models. The schematic view of the proposed FE model for multicell hybrid tubes under axial and oblique loading conditions are presented in **Figure 2**.

A mesh convergence test was performed to obtain more accurate results from the numeric simulations. To this aim, five different element mesh sizes were used as shown in **Figure 3**. As shown in the figure, the optimum results to save computational cost were obtained by using a 1 mm mesh size for lattice structures, and a mesh size of 1 mm for single and multicell tubes.

Energy conservation is an important criterion for determining the reliability of a FE model. The reduced integration method may produce the hourglass mode in the collision simulation, resulting in hourglass energy loss and affecting the system's

energy conservation and simulation accuracy. As a result, it is critical to ensure that the hourglass energy does not exceed 5% of the total energy in order to avoid the hourglass problem.^[41–43] **Figure 4** shows the internal, kinetic, total, and hourglass energies during the crushing process of a selected multicell hybrid tube under impact loading. It is clear that the decrease in kinetic energy is approximately equivalent to the rise in internal energy, and the total energy remains virtually unchanged. As can be seen from **Figure 4**, the hourglass energy is below 1% of the internal energy. Thus, it implies that the model is trustworthy.

2.3.2. Material Properties

The materials of the tube and lattice structure were chosen as Al6063–T5 and AlSi10Mg, respectively. The plastic stress–strain graphs and mechanical properties of the tube and lattice structures are, respectively, shown in **Figure 5** and **Table 2**.

In the FE model, the von Mises-type yield criterion (J2-plasticity) in conjunction with isotropic hardening was used to simulate the plasticity of the materials. It is worth noting that the strain-rate effect is typically ignored for low-velocity impact simulations because aluminum alloys typically exhibit minimal strain-rate sensitivity.^[42,44–46] In the FE modeling, the rate-dependent effect was therefore ignored.

2.3.3. Model Validation

Validation tests were performed to validate the suggested FE model. For experimental validation tests, the β -Ti₃Au lattice structures have five unit cells, a lattice diameter of 2 mm, cross-sectional dimensions of 20 × 20 mm, and a length of 100 mm. Although the length is not particularly long, the specimens' developed fold count is sufficient for the examination of progressive buckling deformation. The lattice structures were manufactured utilizing AlSi10Mg dust particles with a particle size of 30 μ m and the EOS M 290 AM machine. No defects or

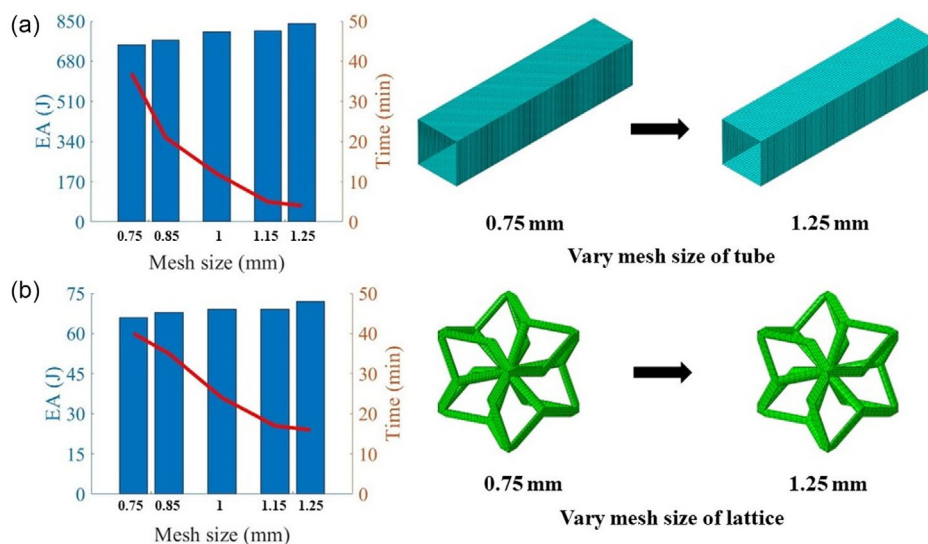


Figure 3. The mesh convergence test results for a) tube and b) lattice structure.

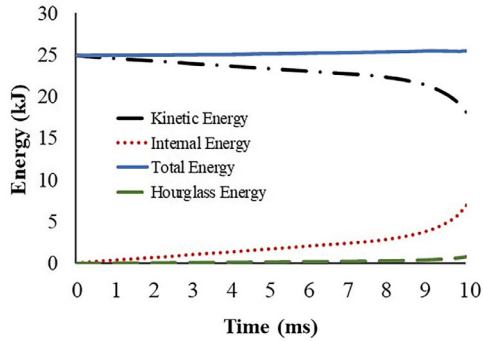


Figure 4. Internal, kinetic, total, and hourglass energies of the multicell hybrid tube.

significant over/undersizing were observed in the lattice structures examined after manufacturing. The supplied 2 mm thick thin-walled tubes were cut into 100 mm lengths, and then the lattice structures were placed inside the tubes to obtain hybrid structures.

Because aluminum alloys have low strain rate sensitivity, the validation tests were conducted at quasistatic conditions, as discussed in the literature studies.^[47,48] The proposed thin-walled tubes were placed between the upper and lower plate of the Shimadzu Autograph AG-IS universal testing machine with a capacity of 100 kN. The quasistatic compression tests were carried out at room temperature and at a speed of 5 mm min⁻¹. A video camera was used to record the crushing process of the tube and hybrid structures. Load and displacement data are collected at a sample rate of 20 points per second.

Although explicit codes are generally used to simulate high-speed impact events, quasistatic situations can also be simulated using explicit codes with reasonable computational time and accuracy.^[49,50] In explicit analysis, time saving can be obtained with some techniques such as speed scale-up and mass scaling. However, there are some points to consider here. For an analysis to be considered as a quasistatic analysis, there are two fundamental requirements. 1) It should be independent of velocity and 2) the total kinetic energy of the structure should be 5% less than the total internal energy.^[51,52] In the current work, in order to best balance between accuracy and computational efficiency, speed scale-up approach was used and the single and multicell tubes were crushed by a rigid plane with a velocity of 1000 mm s⁻¹ in the FE model for simulating quasistatic compression. No additional mass scaling technique was adopted in

Table 2. The mechanical properties of the tube and lattice structures.

Material	E [GPa]	σ_Y [MPa]	ρ [kg m ⁻³]	ν
Al6063-T5 ^[56]	68.2	187	2700	0.33
AlSi10Mg ^[57]	69.3	160	2670	0.30

FE model. The comparison results of kinetic and internal energy for FE model of the tubes are presented in **Figure 6**.

It is clearly seen that the total kinetic energy is less than 5% of the total internal energy. It can be concluded from this that the quasistatic compression process is accurately simulated. The deformation modes comparison of single and hybrid tubes between experimental test and FE simulation is shown in **Figure 7**. It can be seen that the deformation shapes in the FE simulation are quite similar to the test results. **Figure 8** depicts the force–displacement curves of single and hybrid tubes with test and simulation results. **Table 3** shows the findings of their comparison of crashworthiness indicators. Obviously, the force–displacement curve of the experimental test agrees well with the FE simulation curve. Furthermore, the relative errors in crashworthiness indicators between experiment and simulation are all within 5% of one another.

3. Results and Discussion

3.1. Interaction of Lattice Structure with Tube

The difference between the sum of the individual crashworthiness indicators of two separate structures and the crashworthiness indicators of the hybrid structure is defined as the synergistic effect between the two individual constituents.^[53] These synergistic effects contribute to the extra EA of the hybrid structure compared to individual structures and the following equations can be used.

$$EA_{\text{empty tube+lattice}} = EA_{\text{empty tube}} + EA_{\text{lattice}} \quad (6)$$

$$EA_{\text{synergy}} = EA_{\text{hybrid}} - EA_{\text{empty tube+lattice}} \quad (7)$$

$$SEA_{\text{empty tube+lattice}} = \frac{EA_{\text{empty tube}} + EA_{\text{lattice}}}{m_{\text{empty tube}} + m_{\text{lattice}}} \quad (8)$$

$$SEA_{\text{synergy}} = SEA_{\text{hybrid}} - SEA_{\text{empty tube+lattice}} \quad (9)$$

$$MCF_{\text{empty tube+lattice}} = \frac{EA_{\text{empty tube}} + EA_{\text{lattice}}}{\delta} \quad (10)$$

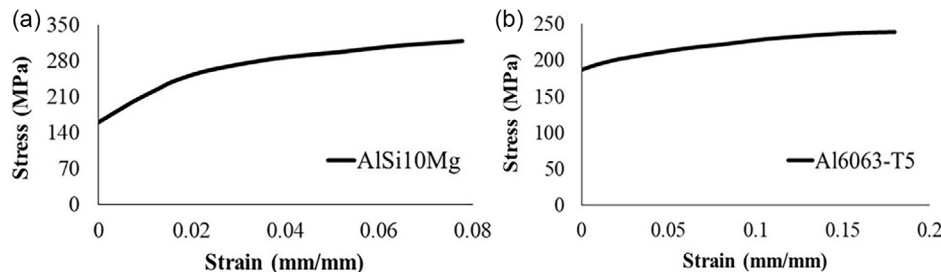


Figure 5. The true plastic stress–strain graphs of a) AlSi10Mg and b) Al6063-T5.

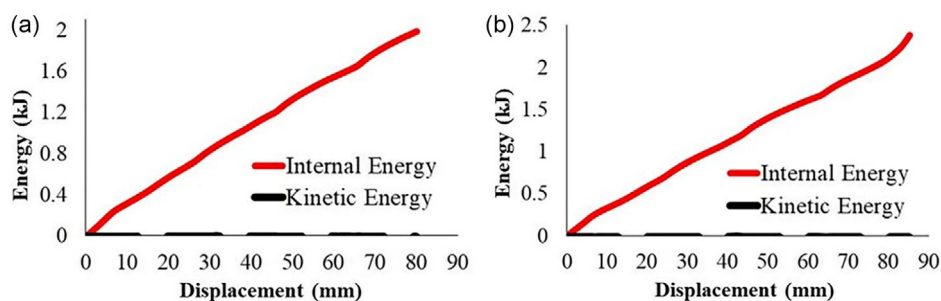


Figure 6. Comparison of kinetic and internal energy for FE model of a) empty tube and b) hybrid tube.

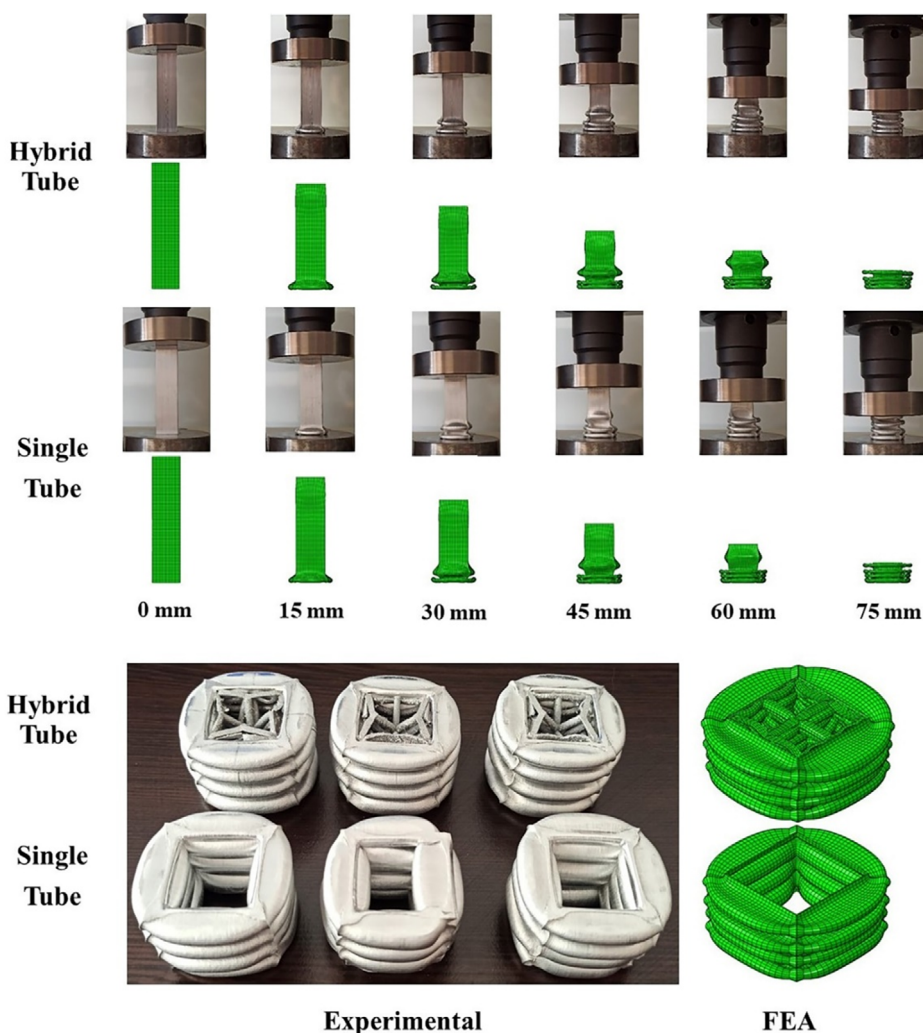


Figure 7. The progressive collapse mode comparison of single and hybrid tubes.

$$MCF_{\text{synergy}} = MCF_{\text{hybrid}} - MCF_{\text{empty tube+lattice}} \quad (11) \quad CFE_{\text{empty tube+lattice}} = \frac{MCF_{\text{empty tube+lattice}}}{PCF_{\text{empty tube+lattice}}} \quad (14)$$

$$PCF_{\text{empty tube+lattice}} = PCF_{\text{empty tube}} + PCF_{\text{lattice}} \quad (12)$$

$$PCF_{\text{synergy}} = PCF_{\text{hybrid}} - PCF_{\text{empty tube+lattice}} \quad (13) \quad CFE_{\text{synergy}} = CFE_{\text{hybrid}} - CFE_{\text{empty tube+lattice}} \quad (15)$$

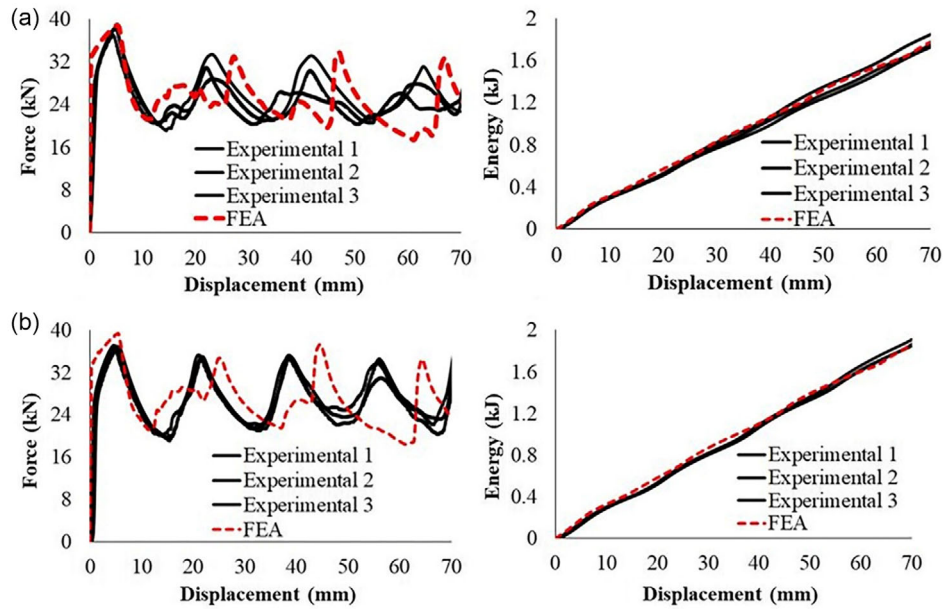


Figure 8. The force–displacement curves comparison of a) single and b) hybrid tubes between experiment and simulation.

Table 3. The EA indicators comparison of single and hybrid tubes between test and simulation.

		EA [J]	SEA [J g ⁻¹]	MCF [kN]	PCF [kN]	CFE
Empty tube	Exp. 1	1727.80	35.82	24.68	37.04	0.67
	Exp. 2	1749.68	36.27	24.99	38.34	0.65
	Exp. 3	1847.03	38.32	26.38	38.31	0.69
	Exp. mean (STD)	1774.84 (63.47)	36.80 (1.33)	25.35 (0.91)	37.90 (0.74)	0.67 (0.02)
	FEA	1778.66	37.45	25.41	38.91	0.65
	Relative error (%)	0.22	1.77	0.24	2.66	2.98
Hybrid tube	Exp. 1	1910.91	32.71	27.30	38.11	0.72
	Exp. 2	1864.49	32.17	26.66	37.87	0.70
	Exp. 3	1851.43	31.85	25.93	37.96	0.68
	Exp. mean (STD)	1875.61 (31.26)	32.24 (0.43)	26.63 (0.69)	37.98 (0.12)	0.70 (0.02)
	FEA	1853.40	32.33	26.48	39.30	0.67
	Relative error (%)	1.18	0.28	0.56	3.47	4.28

Figure 9 shows the synergistic effects by considering the force–displacement and energy–displacement values of tubes having different cell numbers under axial loading condition. As can be seen in the figure, because there are no vertical components, β -Ti₃Au lattice structures have relatively minor force–displacement characteristics with a lengthy plateau and no noticeable peaks. This results in a crushing behavior that is generally continuous and smooth, which is highly comparable to the crushing behavior of foam structures.^[54] As a result, the force–displacement curves for the sum of the lattice structures and empty tubes show tendencies that are comparable to those of the empty tube. The load is moved to the following unit cell when a unit cell is crushed, and the force values drop as the force is transmitted between the cells. When the empty tube with a

tube thickness of 1 mm and the lattice structures with 5 cells and a strut diameter of 2 mm are compared separately, it is seen that the tube structure absorbs much more energy than the lattice structure. The decrease in force values is related to the amount of unit cells in the hybrid structure. However, while the number of cells in the lattice structure is constant, as the number of divided cells in the tube increases, the force values in the structure become more stable with fewer peaks. It is clearly observed from **Figure 9** that as the cell number increases inside the tubes, force and absorbing energy values are increased. Various crashworthiness values of empty tubes, lattice structures, hybrid tubes, and individual sum of lattice structures with empty tubes are presented in **Table 4** for different cell numbers. It is evident that incorporating lattice structures into the multicell tube effectively

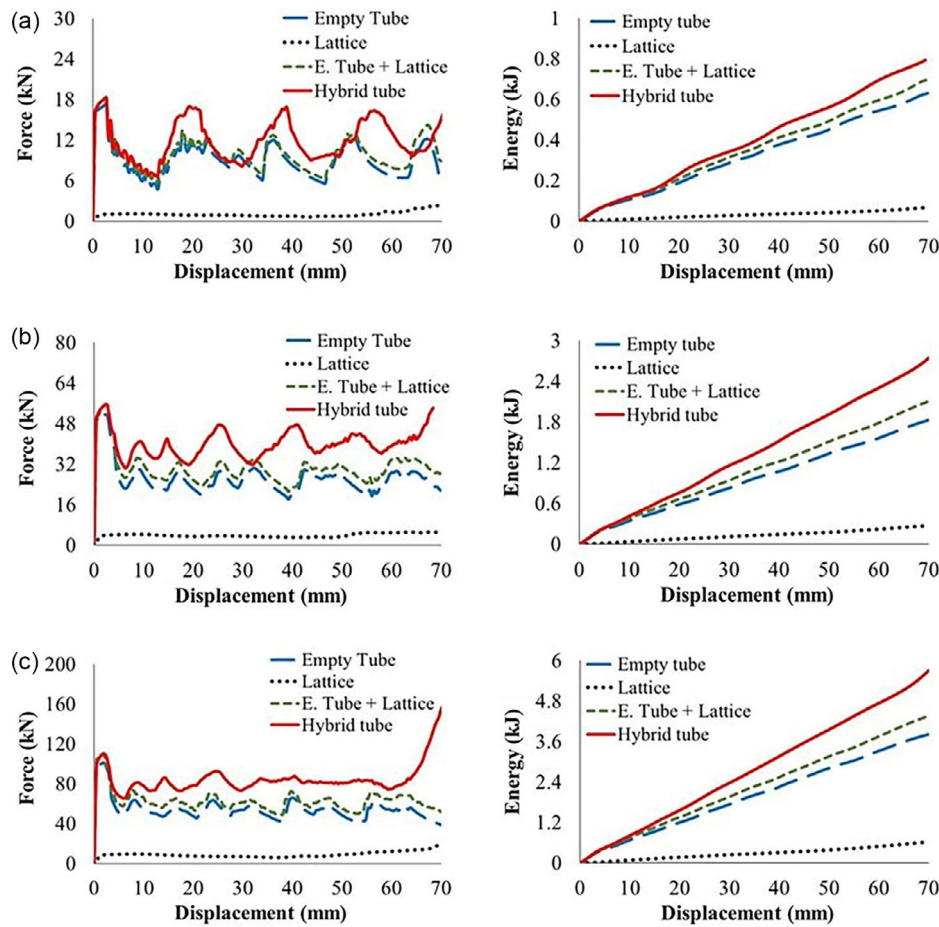


Figure 9. The force–displacement and energy–displacement curves of tubes having different cell numbers: a) 1×1 single, b) 2×2 multicell, and c) 3×3 multicell.

Table 4. Comparison of EA performances of individual tube and lattice structures with hybrid tubes having different cell numbers.

Structure type	EA [J]	Synergistic contribution [%]	Mass [g]	SEA [J g^{-1}]	Synergistic contribution [%]	MCF [kN]	Synergistic contribution [%]	PCF [kN]	Synergistic contribution [%]	CFE	Synergistic contribution [%]
1×1 Empty tube	629.59	–	22.70	27.74	–	8.99	–	17.29	–	0.52	–
	Lattice	69.60	–	9.83	7.08	–	0.99	2.30	–	0.43	–
	Empty tube+Lattice	699.20	–	32.53	21.49	–	9.99	19.59	–	0.51	–
	Hybrid tube	805.12	15.15	32.53	24.75	15.15	11.50	18.26	6.82	0.63	23.58
2×2 Empty tube	1836.27	–	68.00	27.00	–	26.23	–	51.53	–	0.51	–
	Lattice	271.69	–	39.32	6.91	–	3.88	5.75	–	0.67	–
	Empty tube+Lattice	2107.96	–	107.32	19.64	–	30.11	57.28	–	0.53	–
	Hybrid tube	2747.96	30.36	107.32	25.61	30.36	39.26	65.67	–14.64	0.60	13.72
3×3 Empty tube	3811.10	–	136.00	28.02	–	54.44	–	101.22	–	0.54	–
	Lattice	626.36	–	88.47	7.08	–	8.95	19.17	–	0.47	–
	Empty tube+Lattice	4437.46	–	224.47	19.77	–	63.39	120.40	–	0.53	–
	Hybrid tube	5701.39	28.48	224.47	25.40	28.48	81.45	153.67	–27.64	0.53	0.66

enhances crashworthiness in the design process. It should be noted that Figure 9 and Table 4 are presented for 1 mm wall thickness, 2 mm lattice strut diameter value, and 5 cell lattice structure. However, similar curve patterns and synergistic effects are also observed for different thickness, lattice strut diameter, and cell number values. It is obvious from the table that the EA, SEA, MCF, and CFE values for all different multicell hybrid tubes are greater than the sum of those lattice structures and tubes. As the number of tube cells in the multicell hybrid structure increases, CFE values and synergistic contribution rates decrease. The reason for this is that as the number of cells in the multicell structure increases, PCF values also increase significantly.

3.2. Parametric Analysis

The effects of tube cell number, lattice cell number, lattice strut diameter, and tube thickness on structural crashworthiness are investigated in this section using numerical simulations under axial and oblique loading conditions. In this context, the force responses, EA performances, and deformed shapes of the proposed multicell hybrid tubes are examined in this subsection.

3.2.1. Effect of Single and Multicell Tubes on Structural Crashworthiness

The force–displacement curves, deformation shapes, and crashworthiness indices of the single and multicell tubes under different loading conditions are plotted in Figure 10 and 11. Here, number of lattice cell, tube thickness, and lattice strut diameter are selected 5, 0.5, and 2 mm, respectively. Typically, in force–displacement and accordingly stress–strain curves of the thin-walled tubes under axial loading condition have four main regions: elastic, elastic–plastic, plateau, and densification regions. While stress levels rise sharply in the elastic zone, structures begin to deform permanently when force rises in the

elastic–plastic region. Then, in the plateau region, a long smooth curve is generated by the deformation of the elements in the structures one after the other. Finally, in the densification zone, all of the structure’s supporting elements collapse on top of each other. As multicell tubes have elements that can carry more load than single tubes, it is natural that they have more energy capacity. As can be clearly seen from Figure 10, as the number of cells in the tube increases, the force and therefore the energy values of the relevant hybrid tubes increase. Particularly, for axial loading, the energy absorbed by the hybrid structure with 9 cells (3×3) is 126.17% higher than that of the hybrid structure with 4 cells (2×2) and 716.32% more than that of the hybrid tube with 1 cell (1×1). It is clearly seen that as the loading angle increases for both single and multicell structures, the EA performance of the structures decreases. As some of the load in oblique loading condition is spent in horizontal directions,^[55] unsurprisingly, the highest PCF value was realized under axial loads for all structures. While densification is observed in the structure after a certain deformation length under axial and 10° loading angle, densification is not observed as global bending occurs at loadings greater than 10° , which causes a decrease in EA capacity.

As previously stated, multicell tubes offer larger energy capacity because their elements can handle more load than single tubes. Therefore, it should be also examined in terms of absorbed energy per unit mass values (i.e., SEA) and other crashworthiness parameters such as MCF, PCF, and CFE. Comparison of single and multicell tubes under different loading conditions according to various crashworthiness parameters is presented in Figure 11.

When SEA values for single and multicell structures are considered, it is seen that the structure with the highest SEA value for axial loading is the 3×3 hybrid structure, followed by 2×2 and 1×1 structures, respectively. Particularly, under axial conditions, the SEA value of the 3×3 hybrid structure is 5.92% higher than 2×2 and 10.31% higher than 1×1 . While the difference between the SEA value of the 3×3 hybrid structure and

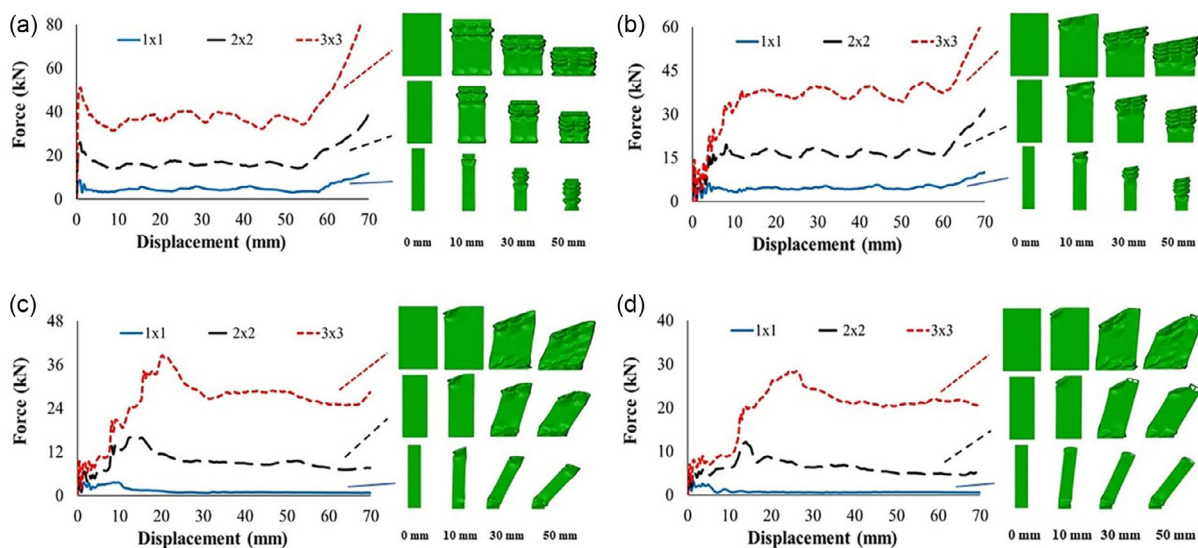


Figure 10. Comparison of force–displacement curves and deformation shapes of tubes having different cell numbers under different loading conditions: a) loading angle of 0° , b) loading angle of 10° , c) loading angle of 20° , and d) loading angle of 30° .

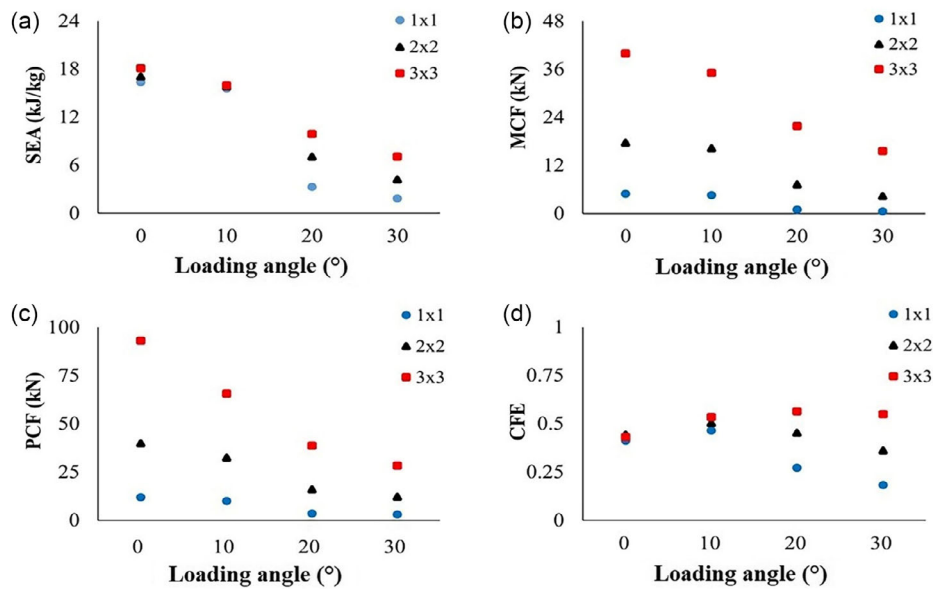


Figure 11. The comparison of tubes having different cell numbers under different loading conditions on various crashworthiness indices a) SEA, b) MCF, c) PCF, and d) CFE.

other structures is small under 10° axial loading conditions, the difference is greater under 20° and 30° loading conditions. The reason for this is that above 10° , both 1×1 and 2×2 multicell structures undergo progressive deformation until a certain deformation length, and then they undergo global buckling. The 3×3 hybrid structure undergoes progressive deformation without showing global buckling even under 30° loading conditions. This situation can also be observed from the deformation shapes in Figure 10. Considering the MCF values, it is seen that the 3×3 hybrid structure is higher than the MCF value of the 2×2 and 1×1 structures for all loading situations. As there is more material to carry the load on the hybrid structure, the increase in the number of cells has resulted in higher MCF values. For all structures, while the MCF value is high due to the ability to use a longer tube length effectively due to local and progressive buckling in axial and 10° loading situations, a dramatic decrease in MCF values is observed after loading angle of 10° due to the global buckling of the structure. The PCF graph also has a very similar trend with the MCF graph, it is seen that the 3×3 hybrid structure is higher than the MCF value of the 2×2 and 1×1 structure for all loading cases. In terms of energy dissipation efficiency, high PCF affects the CFE value. For this reason, it is observed that CFE values are relatively lower for axial loading because the PCF values of structures subjected to axial loading are quite high. The CFE values of single and multicell tubes for axial and loading angle of 10° vary between 0.41 and 0.53.

3.2.2. Effect of Lattice Cell Number on Structural Crashworthiness

The force–displacement curves, deformation shapes, and crashworthiness indices of the multicell tubes having different lattice cell numbers under multiple loading conditions are presented in Figure 12 and 13. Here, number of cell for tube, lattice strut

diameter, and tube thickness are selected 3×3 , 1 mm, and 1.5 mm, respectively.

Multicell hybrid tubes formed by stacking different numbers of lattice unit cells on the same base cross section are presented in Figure 12. As mentioned in Section 2.1, 70% was taken as the CE value for all structures. For this reason, the crushing lengths of hybrid tubes with 4-, 5-, and 6-unit lattice cells with a total tube length of 80, 100, and 120 mm are considered 56, 70, and 84 mm, respectively. It can be seen in the figure that all three structures have similar force–displacement curves. This reveals that the aspect ratio does not have a significant effect for the proposed multicell hybrid tubes. In the study conducted by Cetin and Baykasoğlu^[35] on single hybrid tubes under axial loads, it was revealed that the structures were more prone to global buckling when the number of unit cells increased. Such an effect is not observed in the multicell structures under axial loads in this study. As expected, the highest force and therefore energy value is seen in the axial loading situation, and as the loading angle increases, the force values decrease, for all cases.

As mentioned above, hybrid structures with different lattice unit cells have similar MCF, PCF, and CFE values because they show similar force–displacement curves. However, as the masses of hybrid structures with different unit lattice structures will also differ, there is a slight difference in SEA values. As the heaviest multicell hybrid structure is the 6-cell hybrid structure, the SEA value of the 6-cell hybrid tube is relatively less than that of other hybrid structures in axial and loading angle of 10° .

3.2.3. Effect of Lattice Strut Diameter on Structural Crashworthiness

In this section, the effects of the strut diameter values of the lattice structures placed as filling material in thin-walled multicell tubes on the EA performance of the multicell hybrid structure are

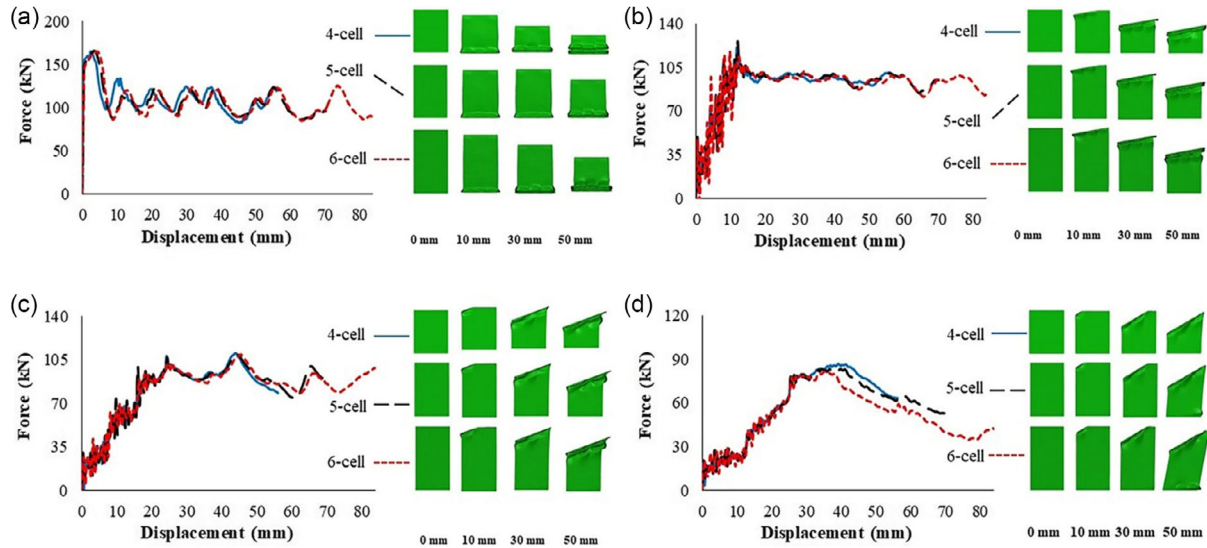


Figure 12. Comparison of force–displacement curves and deformation shapes of tubes having different lattice cell numbers under different loading conditions: a) loading angle of 0°, b) loading angle of 10°, c) loading angle of 20°, and d) loading angle of 30°.

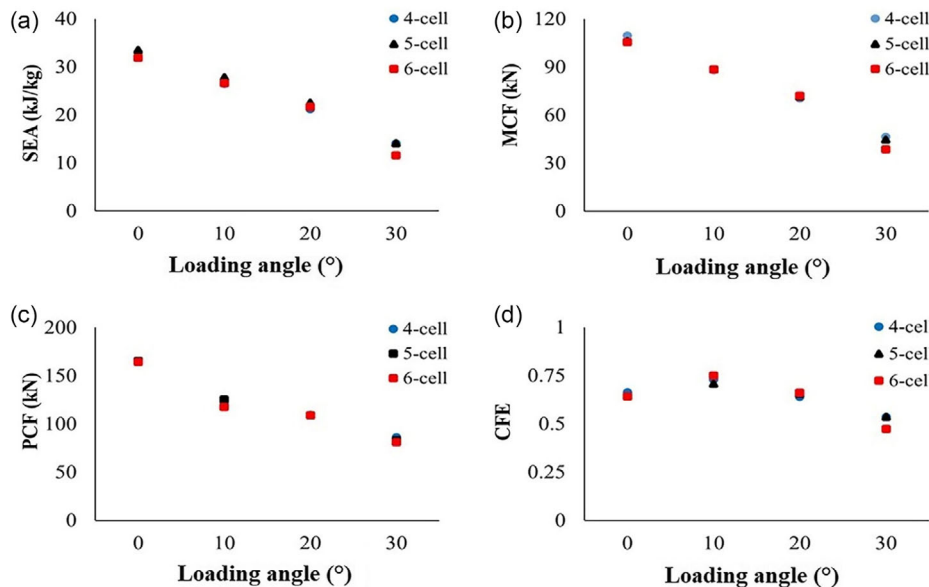


Figure 13. The comparison of tubes having different lattice cell numbers under different loading conditions on various crashworthiness indices: a) SEA, b) MCF, c) PCF, and d) CFE.

examined under various loading conditions. In this context, lattice strut diameter values of 1, 2, and 3 mm are considered and the crashworthiness performances of hybrid structures created with these lattice structures are examined. The force–displacement curves, deformation shapes, and crashworthiness indices of the multicell tubes having different lattice strut diameter under axial and oblique loading conditions are plotted in **Figure 14** and **15**.

Here, number of cell for tube, lattice cell numbers, and tube thickness are selected 3 × 3, 4, and 1 mm, respectively. It can be seen the figure that the structure has highest load capacity in all

three hybrid tube design cases is the hybrid multicell tube with a lattice element diameter of 3 mm. Under axial loading condition, the hybrid tube with a 3 mm lattice strut diameter has about 170% more absorbing energy than the hybrid tube with a 1 mm lattice strut diameter. Under axial and 10° loading conditions, on the other hand, multicell hybrid tubes with a 3 mm lattice strut diameter enter the densification zone earlier, while the hybrid structure with a 1 mm lattice diameter can absorb energy throughout longer deformation. In multicell tubes with a lattice strut diameter of 1 mm, no global buckling is observed during deformation in any loading situation, and a progressive

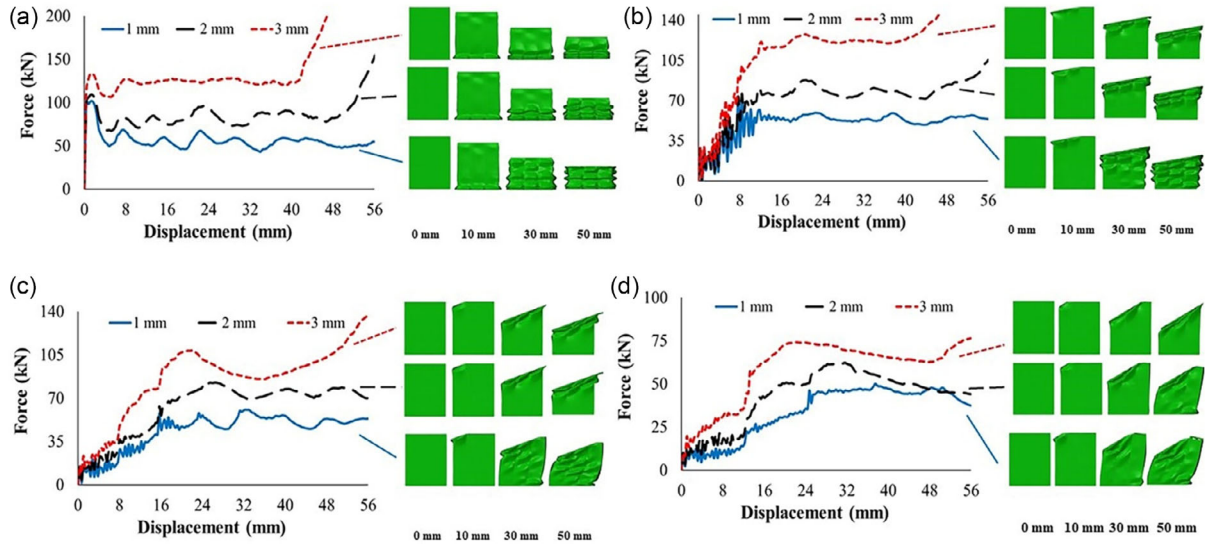


Figure 14. Comparison of force–displacement curves of tubes having different lattice strut diameter under different loading conditions: a) loading angle of 0°, b) loading angle of 10°, c) loading angle of 20°, and d) loading angle of 30°.

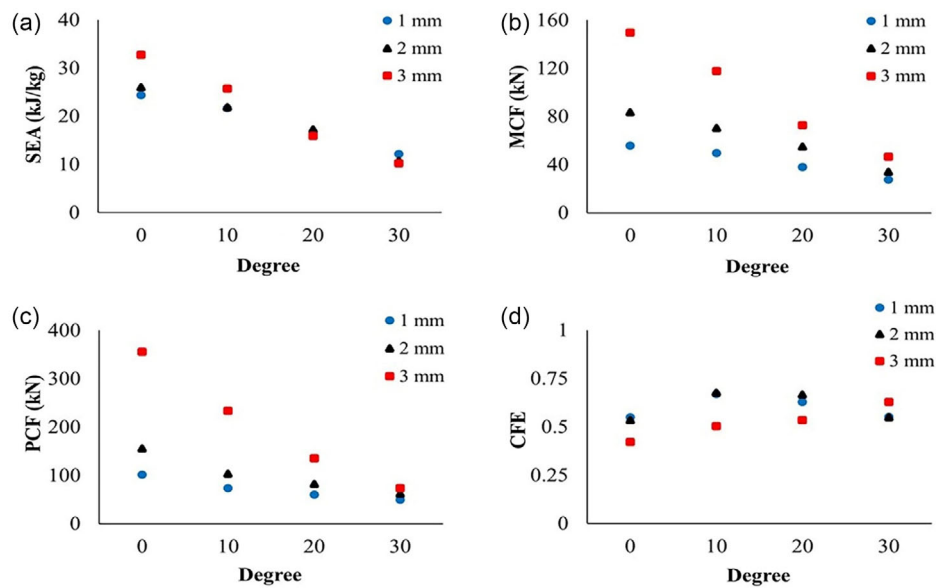


Figure 15. The comparison of having different lattice strut diameter under different loading conditions on various crashworthiness indices: a) SEA, b) MCF, c) PCF, and d) CFE.

deformation behavior is observed along with local buckling. In hybrid tubes with a lattice strut diameter of 2 mm, global buckling is observed only under loading condition of 30° while it behaves with progressive deformation under loading conditions of 0°, 10°, and 20°. On the other hand, global buckling is observed in multicell hybrid tubes with a lattice strut diameter of 3 mm at 20° and 30° loading situations. The MCF value of multicell hybrid tubes with a lattice strut diameter of 3 mm under axial loading is 169.43% higher than the hybrid tube with a lattice strut diameter of 1 mm. However, not surprisingly, its PCF value is considerably higher than other structures due to its high EA capacity.

Therefore, in Figure 15, it can be seen that the CFE value of hybrid tubes with 3 mm lattice strut diameter is lower than those of 1 mm in 0°, 10°, and 20° loading cases.

3.2.4. Effect of Tube Thickness on Structural Crashworthiness

Hybrid structure tube thicknesses are also investigated to determine the influence of tube thickness on EA performance. Three tube thicknesses (0.5, 1, and 1.5 mm) are considered for hybrid multicell tubes. The force–displacement curves, crashworthiness

indices, and deformation shapes of the multicell tubes having different tube thickness under multiple loading conditions are plotted in **Figure 16** and **17**. Here, number of cell for tube, lattice cell numbers, and lattice strut diameter are selected 3×3 , 5, and 2 mm, respectively.

Figure 16 and 17 show that the tube thickness has a dominant effect on the EA capacity of hybrid multicell structures, and the force values of the multicell hybrid tubes increase with the increasing tube thickness for all cases. Furthermore, it is obvious that increasing tube thickness improves the hybrid structures' global buckling resistance, allowing the structure to absorb more impact energy. Multicell hybrid tubes with thinner tube

thicknesses, particularly at high impact angles, have reduced EA capabilities due to global buckling, which can be increased by increasing the tube thickness of the structures. When MCF values are compared, the multicell hybrid tube with 1.5 mm tube thickness has 68.19% more MCF value than the hybrid tube with 1 mm tube thickness and 244.56% more than the hybrid tube with 0.5 mm thickness. This difference is 30.89% and 85.97%, respectively, in terms of SEA. As a result, it is revealed that tube thickness is a significant parameter in the EA behavior of multicell hybrid tubes, and the EA performance of tubes could be improved further by selecting the tube thickness of the hybrid structures appropriately.

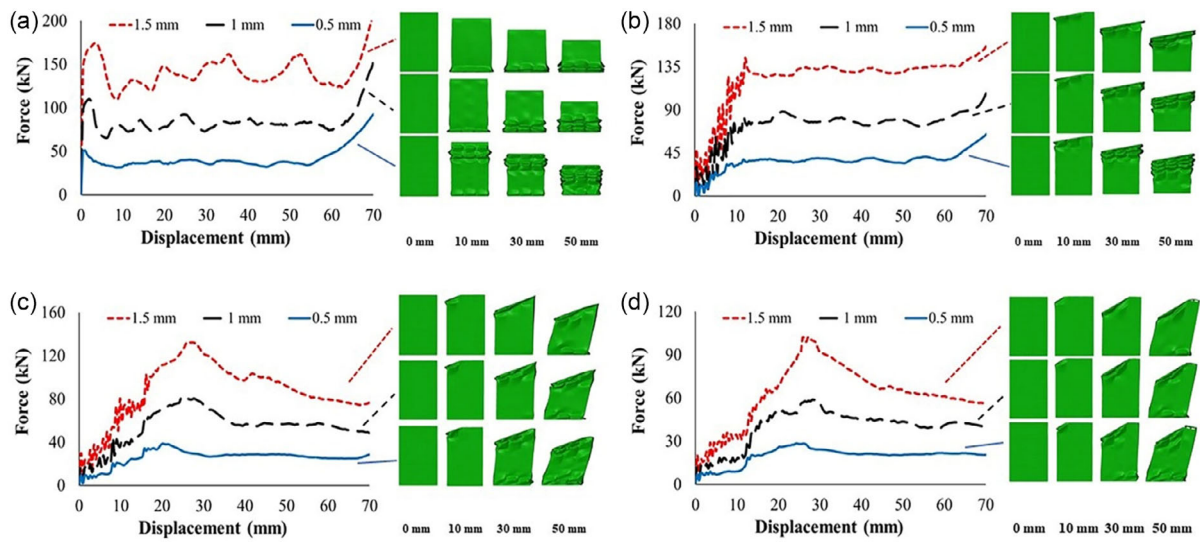


Figure 16. Comparison of force–displacement curves of tubes having different tube thickness under different loading conditions: a) loading angle of 0°, b) loading angle of 10°, c) loading angle of 20°, and d) loading angle of 30°.

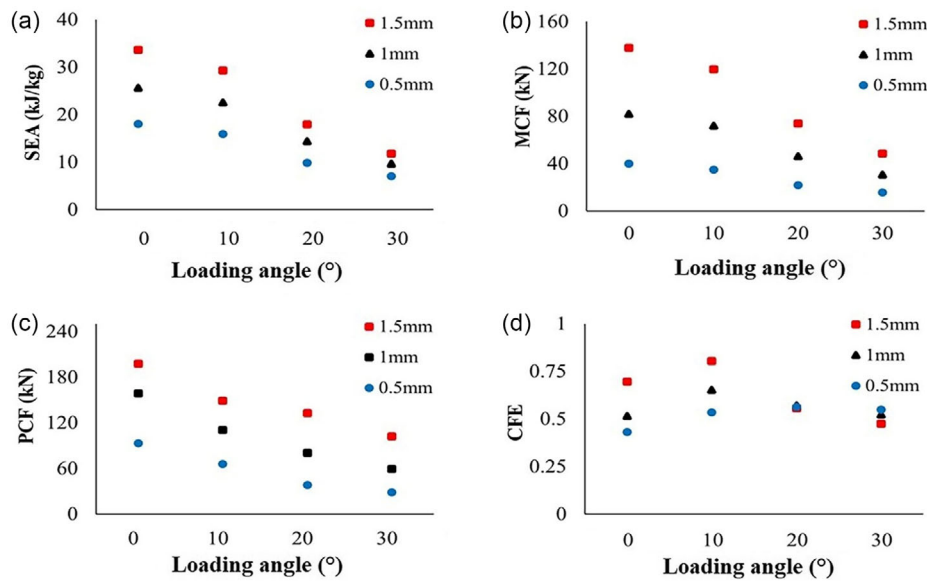


Figure 17. The comparison of having different tube thickness under different loading conditions on various crashworthiness indices: a) SEA, b) MCF, c) PCF, and d) CFE.

4. Conclusion

The present study proposes a novel lattice structure (i.e., β -Ti₃Au geometry)-filled multicell tube, and examines the EA capabilities of these hybrid structures under various impact loading scenarios. Based on validated nonlinear FE analysis, the effects of cell numbers of the tube, numbers of lattice unit cells, lattice strut diameter, and tube thickness on the EA performance of hybrid tubes are investigated in this context. The results showed that the amount of energy absorbed by the hybrid structure was considerably higher than the amount of energy absorbed by the structures individually. This is due to the synergistic effects within the multicell tube and lattice structures. Additionally, the results revealed that the multicell hybrid structure can absorb more energy as the number of compartments within the existing tube increases. Especially as the loading angle increases, the 3×3 structure continues to progressive crushing behavior, while the 1×1 structure is highly prone to global buckling. Moreover, the results showed that the aspect ratio had no significant effect on the proposed multicell hybrid tubes. The results also revealed that as the diameter of the lattice strut in the hybrid tube increases, it creates a positive effect in terms of EA capacity, but on the other hand, the hybrid structure densifies earlier. As another result, it has been revealed that the tube thickness has a dominant effect in terms of the EA capacity of hybrid multicell structures, thus making the structures resistant to global buckling. This study showed that the suitable selection of the proposed filler lattice structure and tube characteristics can significantly improve the crashworthiness of the multicell hybrid tubes.

Acknowledgements

This work was supported by the Scientific Research Projects Governing Unit of Marmara University, project no.: FDK-2022-10482.

Conflict of Interest

The authors declare no conflict of interest.

Author Contributions

Gazi Basar Kocabas: Conceptualization (lead); Investigation (lead); Methodology (lead); Project administration (lead); Resources (lead); Writing—original draft (lead); Writing—review and editing (lead). **Senai Yalcinkaya:** Conceptualization (lead); Funding acquisition (lead); Project administration (lead); Resources (lead); Supervision (lead); Writing—review and editing (lead). **Erhan Cetin:** Investigation (lead); Methodology (lead); Resources (lead); Writing—original draft (lead); Writing—review and editing (lead). **Yusuf Sahin:** Supervision (lead); Writing—review and editing (lead).

Data Availability Statement

The data that support the findings of this study are available on request from the corresponding author. The data are not publicly available due to privacy or ethical restrictions.

Keywords

crashworthiness, finite element methods, lattice structures, multicell tubes, thin-walled tubes

Received: February 26, 2024

Revised: May 20, 2024

Published online:

- [1] N. S. Ha, G. Lu, *Thin-Walled Struct.* **2020**, *157*, 106995.
- [2] A. Baroutaji, M. Sajjia, A. G. Olabi, *Thin-Walled Struct.* **2017**, *118*, 137.
- [3] G. Sun, D. Chen, G. Zhu, Q. Li, *Thin-Walled Struct.* **2022**, *172*, 108760.
- [4] F. Xu, X. Zhang, H. Zhang, *Eng. Struct.* **2018**, *171*, 309.
- [5] S. R. Guillow, G. Lu, R. H. Grzebieta, *Int. J. Mech. Sci.* **2001**, *43*, 2103.
- [6] Ø. Fyllingen, O. S. Hopperstad, M. Langseth, *Int. J. Impact Eng.* **2007**, *34*, 1619.
- [7] Z. Bai, J. Liu, F. Zhu, F. Wang, B. Jiang, *Int. J. Crashworthiness* **2015**, *20*, 401.
- [8] Y. Liu, M. L. Day, *Int. J. Crashworthiness* **2007**, *12*, 503.
- [9] Q. Liu, H. Xing, Y. Ju, Z. Ou, Q. Li, *Compos. Struct.* **2014**, *117*, 1.
- [10] W. Hou, X. Xu, L. Sang, L. Tong, *Thin-Walled Struct.* **2020**, *154*, 106815.
- [11] H. Zhang, X. Zhang, *Thin-Walled Struct.* **2016**, *99*, 35.
- [12] Z. Gao, D. Ruan, *Eng. Struct.* **2023**, *286*, 116141.
- [13] B. Zhou, H. Zhang, S. Han, X. Ji, *Structures* **2024**, *59*, 105827.
- [14] C. Baykasoğlu, A. Baykasoğlu, E. Cetin, *Int. J. Crashworthiness* **2023**, *29*, 80.
- [15] E. Cetin, A. Baykasoğlu, M. E. Erdin, C. Baykasoğlu, *Thin-Walled Struct.* **2023**, *182*, 110321.
- [16] N. A. Z. Abdullah, M. S. M. Sani, M. S. Salwani, N. A. Husain, *Thin-Walled Struct.* **2020**, *153*, 106795.
- [17] Y. Bai, J. Gao, C. Huang, Y. Li, *Chin. J. Mech. Eng.* **2023**, *36*, 143.
- [18] C. Tao, Z. Wang, Z. Liu, Y. Wang, X. Zhou, X. Liang, H. Li, *Aerospace* **2023**, *10*, 524.
- [19] M. Yang, B. Han, Y. Mao, J. Zhang, T. J. Lu, *Thin-Walled Struct.* **2022**, *179*, 109677.
- [20] Y. Liu, Q. Tan, H. Lin, J. Wang, K. Wang, Y. Peng, S. Yao, *Compos. Sci. Technol.* **2023**, *243*, 110252.
- [21] M. A. Güler, S. K. Mert, M. Altin, E. Acar, *J. Braz. Soc. Mech. Sci. Eng.* **2023**, *45*, 541.
- [22] H. Liu, Z. X. C. Chng, G. Wang, B. F. Ng, *Int. J. Mech. Sci.* **2021**, *210*, 106731.
- [23] G. M. M. Nagel, D. P. P. Thambiratnam, *Int. J. Impact Eng.* **2006**, *32*, 1595.
- [24] H. Liang, B. Liu, Y. Pu, H. Sun, D. Wang, *Int. J. Mech. Sci.* **2024**, *266*, 108959.
- [25] N. S. Ha, T. M. Pham, W. Chen, H. Hao, *Int. J. Mech. Sci.* **2023**, *251*, 108260.
- [26] H. Zeng, W. Shi, H. Lv, N. Qiu, C. Ma, Q. Gao, *Thin-Walled Struct.* **2023**, *192*, 111160.
- [27] P. Huo, X. Fan, X. Yang, H. Huang, J. Li, S. Xu, *Latin Am. J. Solids Struct.* **2021**, *18*. <https://doi.org/10.1590/1679-78256406>.
- [28] G. Li, F. Xu, G. Sun, Q. Li, *Int. J. Impact Eng.* **2015**, *77*, 68.
- [29] G. B. Kocabas, E. Cetin, S. Yalcinkayakaya, Y. Sahin, *Int. J. Automot. Sci. Technol.* **2023**, *7*, 207.
- [30] M. Tunay, E. Cetin, *J. Braz. Soc. Mech. Sci. Eng.* **2023**, *45*, 500.
- [31] C. Baykasoğlu, A. Baykasoğlu, M. E. Erdin, E. Cetin, *Polym. Compos.* **2024**, *45*, 5504.
- [32] M. Qi-hua, D. Fan, G. Xue-hui, Z. Tianjun, *Mech. Adv. Mater. Struct.* **2022**, *30*, 2953.
- [33] Y. Zha, Q. Ma, X. Gan, M. Cai, T. Zhou, *Polym. Compos.* **2020**, *41*, 4602.

- [34] C. Bai, Q. Ma, X. Gan, T. Zhou, *Polym. Compos.* **2021**, 42, 5035.
- [35] E. Cetin, C. Baykasoğlu, *Int. J. Mech. Sci.* **2019**, 158, 471.
- [36] E. Svanidze, T. Besara, M. F. Ozaydin, C. S. Tiwary, J. K. Wang, S. Radhakrishnan, S. Mani, Y. Xin, K. Han, H. Liang, T. Siegrist, P. M. Ajayan, E. Morosan, *Sci. Adv.* **2016**, 2, e1600319.
- [37] C. C. Lukose, I. Anastopoulos, T. Mantso, L. Bowen, M. I. Panayiotidis, M. Birkett, *Bioact. Mater.* **2022**, 15, 426.
- [38] Z. Tang, S. Liu, Z. Zhang, *Thin-Walled Struct.* **2013**, 62, 75.
- [39] Z. Zhang, S. Liu, Z. Tang, *Thin-Walled Struct.* **2010**, 48, 9.
- [40] H. Yin, G. Wen, Z. Liu, Q. Qing, *Thin-Walled Struct.* **2014**, 75, 8.
- [41] S. Xu, W. Li, L. Li, T. Li, C. Ma, *Comput. Model. Eng. Sci.* **2022**, 131, 929.
- [42] Y. Zhang, X. Xu, G. Sun, X. Lai, Q. Li, *Thin-Walled Struct.* **2018**, 122, 193.
- [43] C. Wang, Y. Li, W. Zhao, S. Zou, G. Zhou, Y. Wang, *Int. J. Mech. Sci.* **2018**, 138–139, 489.
- [44] V. Espeseth, T. Børvik, O. S. Hopperstad, *Int. J. Impact Eng.* **2022**, 167, 104261.
- [45] W. Wen, M. Lei, Y. Tao, Y. Lian, *Thin-Walled Struct.* **2022**, 176, 109347.
- [46] C. Tao, X. Zhou, Z. Liu, X. Liang, W. Zhou, H. Li, *Materials* **2023**, 16, 1871.
- [47] H. Nikkhah, A. Baroutaji, A. G. Olabi, *Thin-Walled Struct.* **2019**, 142, 132.
- [48] D. Sharma, S. S. Hiremath, *J. Mater. Res. Technol.* **2023**, 23, 3790.
- [49] H. R. Zarei, A. Ghamarian, *Exp. Mech.* **2014**, 54, 115.
- [50] A. Khalkhali, A. Masoumi, A. Darvizeh, M. Jafari, A. Shiri, *J. Mech.* **2011**, 27, 585.
- [51] A. Baroutaji, M. D. Gilchrist, D. Smyth, A. G. Olabi, *Int. J. Impact Eng.* **2015**, 82, 74.
- [52] E. Cetin, C. Baykasoğlu, *Thin-Walled Struct.* **2020**, 154, 106849.
- [53] J. Wang, Y. Zhang, N. He, C. H. Wang, *Mater. Des.* **2018**, 144, 229.
- [54] L. J. Gibson, M. F. F. Ashby, in *Cellular Solids: Structure and Properties*, 1st ed., Cambridge University Press, Cambridge, UK **1997**.
- [55] W. Li, H. Fan, *Int. J. Steel Struct.* **2021**, 21, 202.
- [56] D. Karagiozova, G. N. Nurick, S. Chung Kim Yuen, *Thin-Walled Struct.* **2005**, 43, 956.
- [57] Y. Zhang, T. Liu, H. Ren, I. Maskery, I. Ashcroft, *Compos. Struct.* **2018**, 195, 45.